Nonequilibrium initial conditions of a Brownian oscillator system observed by two-dimensional spectroscopy

Yoko Suzuki and Yoshitaka Tanimura
Institute for Molecular Science, Myodaiji, Okazaki 444-8585, Japan

(Received 21 February 2001; accepted 26 April 2001)

We study effects of a nonequilibrium initial condition of a Brownian oscillator system upon two-, three-, and four-time correlation functions of an oscillator coordinate as a subject of multidimensional spectroscopy. A nonequilibrium initial condition is set by a displacement of a Gaussian wave packet in an oscillator potential. Such situation may be found in a vibrational motion of molecules after a sudden bond breaking between a fragmental molecule and a targeting vibrational system or a movement of wave packet in an electronic excited state potential surface created by a laser pump pulse. Multitime correlation functions of oscillator coordinates for a nonequilibrium initial condition are calculated analytically with the use of generating functional from a path integral approach. Two-, three-, and four-time correlation functions of oscillator coordinates correspond to the third-, fifth-, and seventh-order Raman signals or the first-, second-, and third-order infrared signals. We plotted these correlation functions as a signal in multidimensional spectroscopy. The profile of the signal depends on the initial position and momentum of the wave packet in the fifth- and seventh-order Raman or the second and third order infrared measurement, which makes it possible to measure the dynamics of the wave packet directly in the phase space by optical means. © *2001 American Institute of Physics.*
[DOI: 10.1063/1.1379768]

I. INTRODUCTION

The vibrational mode of molecules in condensed phases has been studied in many experimental and theoretical works. Femtosecond nonlinear optical spectroscopes are powerful tools to obtain information about a variety of dynamic processes, including such important processes as microscopic dynamics, intermolecular couplings, and time scales of solvent evolution that modulate the energy of a transition. However, since vibrational lines from these processes are often broadened and also appear in similar positions, it is not easy to distinguish them from linear spectroscopy. This difficulty can be overcome by higher-order nonlinear optical processes involving many laser interactions. Two-dimensional Raman spectroscopy and two-dimensional infrared spectroscopy are such examples.[1,2] Many experimental efforts along this line of research have been made to probe inhomogeneity of liquids and inter- and intramolecular vibrational motion.[3–7] The 2D information content of these time domain experiments can also be obtained from a frequency domain experiment, and also demonstrated that vibrational interactions in liquids can be observed.[8–12] It is obvious that higher-order spectroscopy can contain many time intervals and these can be used to separate the mechanism of dynamical processes from the others. Theories so far developed are to access various dynamical information for instance the degree of inhomogeneous broadening,[1,13–15] the anharmonicity of potentials and the nonlinearity of polarizability,[16–21] the coupling mechanism between different vibrational modes[22–26] and the structural information of large molecules.[27,28] In this paper, we aim to demonstrate that multidimensional spectroscopy is useful not only to investigate the targeting dynamical processes but also to elucidate information about a difference for an initial distribution of vibrational modes. For the purposes of this work, we consider a Gaussian wave packet in the harmonic vibrational mode, whose center is shifted from the equilibrium position, as an initial condition. Such initial condition may arise from a sudden bond breaking between a fragmental molecule and a targeting vibrational system. A possible example is the ''reaction driven'' coherence in MbNO where the pump pulse creates the reactant excited state (MbNO*), which rapidly decays to Mb+NO [Fig. 1(a)].[29] One may also find similar situation in a movement of a wave packet created in an electronic excited state by a laser pump pulse [Fig. 1(b)]. Displacement and movement of the wave packet is usually observed by the time-dependent emission or absorption spectrum. For example, in a displaced oscillator case, such effects can be seen by the so called dynamical Stokes shift. In some case, however, such measurements are very difficult, since the emission or absorption spectrum is often broadened and featureless from a convolution of all the dynamical and static information within it.

One-dimensional (1D) spectroscopy does not allow unique extraction of information for superimposed dynamical time scales. Multidimensional spectroscopy, which measures the magnitude of a dipole moment or a nonlinear polarization as a function of the two independent coherence evolution periods, can provide more information about the molecular structure and dynamics than 1D spectroscopy. Here we demonstrate a possibility to use multidimensional spectroscopy to probe the nature of the initial distribution. For this purpose, we employ a Brownian oscillator model for

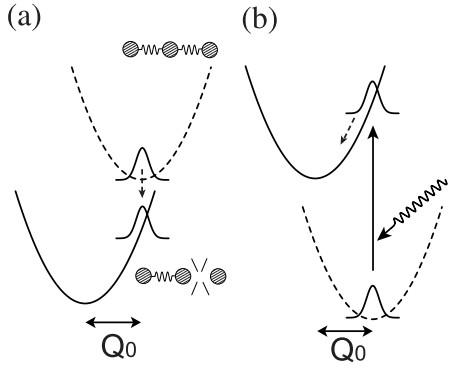

FIG. 1. Schematic view of a creation of nonequilibrim initial condition at $t=t_I$. Example (a) shows the case of a sudden bond breaking between a fragmental molecule and a targeting vibrational system at $t=t_I$. In this situation, the reactant excited state rapidly decays to the ground state and then the wave packet is created in the ground state at $t=t_I$. Example (b) shows the situation in which a wave packet is created in an excited state by a resonant pulse at $t=t_I$.

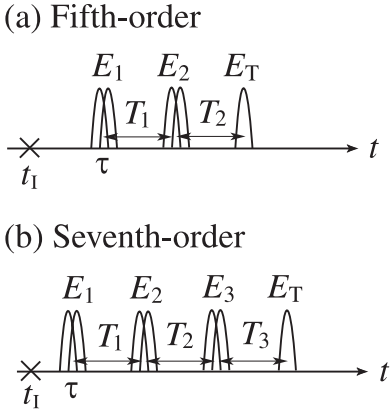

FIG. 2. Pulse configuration for (a) the fifth- and (b) the seventh-order off-resonant Raman experiments. The nonequilibrium initial condition is created at $t=t_I$. Then the movement of the wave packet is detected by a following sequence of pulses, i.e., two or three pairs of pulses are applied to the system, which followed by the last probe pulse. Here the first pair of pulses interact with the system at $t=\tau$. In this paper, the temporal profiles of pulses E_1, E_2, E_3, and E_T are assumed to be impulsive, and are given by (a) Eq. (2.5) and (b) Eq. (2.6).

a molecular vibrational mode and incorporate the displacement of the initial distribution into the Brownian motion theory using nonequilibrium generating functional calculated from a path integral approach. We reformulate optical response functions expressed by time correlation functions of the molecular polarizability or the dipole moment and obtain their analytical expressions which are the observable of multidimensional Raman or infrared spectroscopy.

In Sec. II, the $(2N+1)$th order Raman and Nth order infrared signals are described to arbitrary order in terms of response functions which are expressed by multitime correlation functions of polarizability or dipole moment. In Sec. III, we show any order of response function can be expressed by a generating functional whose calculational details are shown in Appendix A. We then calculated the response functions analytically with the use of the diagrammatical rule described in Appendix B. The numerical results are presented in Sec. IV and finally conclusions are given in Sec. V.

II. RESPONSE FUNCTIONS FOR HIGHER-ORDER OPTICAL PROCESSES

We consider a molecular system in the condensed phase which is subjected to laser pulses. If the system is described by a single oscillation mode specified by its coordinate $\hat{Q}$ and momentum $\hat{P}$, the total Hamiltonian of the system and the bath is written as

$$\hat{H}=\frac{\hat{P}^2}{2M}+\frac{1}{2}M\Omega^2\hat{Q}^2 + \sum_i \left\{ \frac{\hat{p}_i^2}{2m_i}+\frac{m_i\omega_i^2}{2}\left(\hat{q}_i-\frac{c_i\hat{Q}}{m_i\omega_i^2}\right)^2\right\}. \tag{2.1}$$

Here, Ω denotes the oscillator frequency. The coordinate, conjugated momentum, mass, and frequency of an ith oscillator are given by $\hat{q}_i$, $\hat{p}_i$, m_i, and ω_i, respectively. The interaction between the system and the ith oscillator is assumed to be $\hat{H}_{\mathrm{SB}}=-c_i\hat{q}_i\hat{Q}$. The term $\Sigma_i c_i^2\hat{Q}^2/(2m_i\omega_i^2)$ is a counter term which cancels the unphysical divergence from the coupling to the bath degrees of freedom. The summation over i goes to infinity in order to describe the dissipation on the molecular system.

We consider optical measurements where the molecular system is interacting with a laser field, $E(t)$. For off-resonant Raman spectroscopy, in which resonance arises from a pair of laser pulses through Raman excitation processes, the effective Hamiltonian is given by

$$\hat{H}_{\mathrm{Raman}}=\hat{H}-E^2(t)\alpha(\hat{Q}), \tag{2.2}$$

where $\alpha(\hat{Q})$ is the coordinate dependent Raman polarizability. For resonant IR spectroscopy, the Hamiltonian including laser interaction is given by

$$\hat{H}_{\mathrm{IR}}=\hat{H}-E(t)\mu(\hat{Q}), \tag{2.3}$$

where $\mu(\hat{Q})$ is the coordinate dependent dipole moment. As both Raman polarizability and dipole moment can be expanded as $\alpha(\hat{Q})=\alpha_0+\alpha_1\hat{Q}+\alpha_2\hat{Q}^2/2+\cdots$, or $\mu(\hat{Q})=\mu_0+\mu_1\hat{Q}+\alpha_2\hat{Q}^2/2$, the optical responses of Raman and resonant IR are formally identical besides the fact that the $(2N+1)$th-order Raman spectroscopy corresponds to the Nth order IR spectroscopy. Therefore, hereafter we do not distinguish between the Nth-order IR and $(2N+1)$th-order Raman processes and present only the results for Raman spectroscopy. Notice however that the even-order of IR response signals vanish for isotropic material.

In the $2N+1$th order off-resonant Raman experiment, the signal contributions are from Raman excitation that occurs while Raman pulse pairs are temporally overlapped. Thus each interaction occurs with a time coincident pulse pair. Also, the polarization detected is temporally overlapped with the probe pulse. The pulse configurations for (i) third-, (ii) fifth-, and (iii) seventh-order processes are described as (see Fig. 2)

$$\text{(i)}\quad E_1(t)=\delta(t-\tau),\quad E_T(t)=\delta(t-T_1-\tau), \tag{2.4}$$

$$\text{(ii)}\quad E_1(t)=\delta(t-\tau),\quad E_2(t)=\delta(t-T_1-\tau),$$
$$E_T(t)=\delta(t-T_1-T_2-\tau), \tag{2.5}$$
$$\text{(iii)}\quad E_1(t)=\delta(t-\tau),\quad E_2(t)=\delta(t-T_1-\tau),$$
$$E_3(t)=\delta(t-T_1-T_2-\tau),$$
$$E_T(t)=\delta(t-T_1-T_2-T_3-\tau). \tag{2.6}$$

Here we have assumed that laser pulses are impulsive. The pump pulses and the probe pulse have been written as $E_j(t)$ $(j=1,2,\ldots,N)$ and $E_T(t)$, respectively. The Raman signals for the optically heterodyned detection are expressed by the response functions as

$$I^{(2N+1)}(T_1,T_2,\ldots,T_N;\tau)\propto R^{(2N+1)}(T_N,\ldots,T_2,T_1;\tau), \tag{2.7}$$

which are the N time correlation functions of the polarizability operator $\alpha(\hat{Q})$ given in terms of

$$R^{(2N+1)}(T_N,\ldots,T_2,T_1;\tau)$$
$$=\left(\frac{i}{\hbar}\right)^N\langle[[[\cdots[\hat{\alpha}(T_1+T_2+\cdots+T_N+\tau),$$
$$\hat{\alpha}(T_1+T_2+\cdots+T_{N-1}+\tau)],\ldots],\hat{\alpha}(T_1+\tau)],\hat{\alpha}(\tau)]\rangle, \tag{2.8}$$

where $\hat{\alpha}(t)$ represents the Heisenberg operator given by $\hat{\alpha}(t)=e^{(i/\hbar)\hat{H}t}\alpha(\hat{Q})e^{-(i/\hbar)\hat{H}t}$ and $\langle\cdots\rangle$ means the expectation value of "$\cdots$" defined by $\langle\cdots\rangle=\mathrm{Tr}\{\rho_I\cdots\}/\mathrm{Tr}\{\rho_I\}$ in which ρ_I implies an initial density matrix. Notice that ρ_I is chosen as the nonequilibrium density matrix in the present study, so that correlation functions are not stationary, i.e., $\langle[\hat{\alpha}(t+t'),\hat{\alpha}(t)]\rangle\neq\langle[\hat{\alpha}(t'),\hat{\alpha}(0)]\rangle$.

III. GENERATING FUNCTIONAL IN NONEQUILIBRIUM PROCESS

A generating functional is defined as a functional of the external force which is obtained from the density matrix by tracing over all degrees of freedom of the total system. It is convenient to calculate the higher-order response functions which are derived by performing the functional differentiation in terms of the external force. To calculate the generating functional, we need to trace out the system and bath degrees of freedom. The path integral method is suitable to carry out such procedure. In this section, we demonstrate how to apply the generating functional formalism to the calculation of the higher-order response function.

Let us introduce the sources $J(t)$ and $K(t)$ coupled to $\hat{Q}$ and $\alpha(\hat{Q})$,

$$\hat{H}_{J,K}(t)=\hat{H}-J(t)\hat{Q}-K(t)\alpha(\hat{Q}). \tag{3.1}$$

The generating functional $W[J,K]$ is then defined by

$$\exp\left(\frac{i}{\hbar}W[J,K]\right)=\mathrm{Tr}(\hat{U}_{J_1,K_1}(\infty,t_I)\hat{\rho}_I\hat{U}^{\dagger}_{J_2,K_2}(\infty,t_I))$$
$$=\int dQ_I\int dQ_I'\int d\mathbf{q}_I\int d\mathbf{q}_I'\langle Q_I'\mathbf{q}_I'|$$
$$\times\hat{\rho}_I|Q_I\mathbf{q}_I\rangle\langle Q_I\mathbf{q}_I|\hat{U}^{\dagger}_{J_2,K_2}(\infty,t_I)$$
$$\times\hat{U}_{J_1,K_1}(\infty,t_I)|Q_I'\mathbf{q}_I'\rangle, \tag{3.2}$$

where

$$\hat{U}_{J_\alpha,K_\alpha}(\infty,t_I)=\mathrm{T}\exp\left(-\frac{i}{\hbar}\int_{t_I}^{\infty}dt\hat{H}_{J_\alpha,K_\alpha}(t)\right), \tag{3.3}$$

and $\hat{U}^{\dagger}_{J,K}$ is the adjoint of $\hat{U}_{J,K}$. The symbol T implies the time ordering operator. The real time paths are represented by suffix $\alpha=1,2$ and the sources J_1 and K_1 are for the left-hand side time evolution kernel, whereas J_2 and K_2 are the right. The matrix $\hat{\rho}_I$ is an arbitrary density operator at the initial time t_I which does not need to be an equilibrium distribution. In the second line of Eq. (3.2), we have inserted the completeness relation for the basis $\{|Q_I,\mathbf{q}_I\rangle\}$: $1=\int dQ_I\int d\mathbf{q}_I|Q_I,\mathbf{q}_I\rangle\langle Q_I,\mathbf{q}_I|$. The $(2N+1)$th order response function is given by the differentiation of the generating functional $W[J,K]$ as follows:

$$R^{(2N+1)}(T_N,\ldots,T_2,T_1;\tau)$$
$$=\theta(T_1)\theta(T_2)\cdots\theta(T_N)\left(\frac{i}{\hbar}\right)^N G_R^{(N+1)}(t_0,t_1,t_2,\ldots,t_N), \tag{3.4}$$

$$G_R^{(N+1)}(t_0,t_1,t_2,\ldots,t_N)$$
$$\equiv\left(\frac{\hbar}{i}\right)^N\left(\frac{\delta^{N+1}W[J,K]}{\delta K_-(t_0)\delta K_+(t_1)\delta K_+(t_2)\cdots\delta K_+(t_N)}\right)_{K=0,J=0}, \tag{3.5}$$

where we set $t_i\equiv\tau+T_1+T_2+\cdots+T_{N-i}$ (for $i=0,1,\ldots,N-1$), $t_N\equiv\tau$, and

$$K_+(t)=\frac{K_1(t)+K_2(t)}{2},\quad K_-(t)=K_1(t)-K_2(t). \tag{3.6}$$

From Eq. (3.5), we can systematically derive the higher-order response functions, once we obtain the generating functional. We assume that the system and the bath are initially factorized. Consequently the factor $\langle Q_I'q_I'|\hat{\rho}_I|Q_Iq_I\rangle$ in Eq. (3.2) can be expressed as the product of the system part and the bath part,

$$\langle Q_I'q_I'|\hat{\rho}_I|Q_Iq_I\rangle=\langle Q_I'|\hat{\rho}_I^{(S)}|Q_I\rangle\langle q_I'|\hat{\rho}_I^{(B)}|q_I\rangle. \tag{3.7}$$

We further assume the bath is in the equilibrium state,

$$\hat{\rho}_I^{(B)}=\frac{\exp(-\beta\hat{H}_B)}{\mathrm{Tr}_B\exp(-\beta\hat{H}_B)}, \tag{3.8}$$

where

$$\hat{H}_B=\sum_i\left\{\frac{\hat{p}_i^2}{2m_i}+\frac{m_i\omega_i^2}{2}\hat{q}_i^2\right\}, \tag{3.9}$$

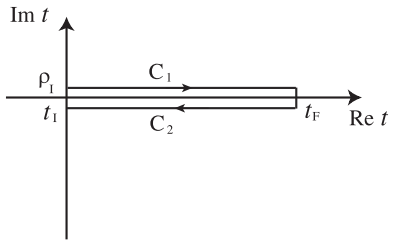

FIG. 3. Contour paths C_1, C_2.

and Tr_B denotes the trace over the bath coordinates. As mentioned in Sec. I, we consider the case where the initial state of the system is set by the displaced Gaussian wave packet given by

$$\langle Q_I'|\hat{\rho}_I^S|Q_I\rangle=\left(\frac{2a}{\pi}\right)^{1/2}\mathrm{e}^{-a(Q_I-Q_0)^2-a(Q_I'-Q_0)^2}, \tag{3.10}$$

where Q_0 is the displacement from the bottom of the harmonic potential and $1/a$ is the width of the initial wave packet. We introduce the contour path for time integration to write various formulas in a compact way.[30–32] The contour time integral $\int_C dt$ runs from C_1 to C_2 defined by $C_1: t_I \to\infty$ and $C_2: \infty\to t_I$ (return path) (see Fig. 3). The path integral method allows us to obtain the analytical expression of the generating functional $W[J,K]$ of the Brownian motion model even for the strong system–bath coupling and the heat bath with a finite correlation time. The detailed derivation of $W[J,K]$ with the aid of the path integral is shown in Appendix A. By using the notation

$$J_+(t)=\frac{J_1(t)+J_2(t)}{2},\quad J_-(t)=J_1(t)-J_2(t), \tag{3.11}$$

the generating functional for $\alpha(\hat{Q})=\alpha_1\hat{Q}+\alpha_2\hat{Q}^2/2+\cdots$ is written as

$$\exp\left(\frac{i}{\hbar}W[J,K]\right)=\exp\left(\frac{i}{\hbar}W[J=K=0]\right)\times\exp\left(\frac{i}{\hbar}S_1[J,K;\delta/\delta\varphi]\right)\times\exp\left(\frac{i}{\hbar}S_2[K,\varphi]\right)\Big|_{\varphi=0,J=0}, \tag{3.12}$$

where

$$S_1[J,K;\delta/\delta\varphi]=\frac{i}{\hbar}\int_{t_I}^{\infty}dt\int_{t_I}^{\infty}dt'\left\{\left(\frac{\hbar}{i}\frac{\delta}{\delta\varphi_+(t)}+J_-(t)+\alpha_1K_-(t)\right)\times K^{(+-)}(t-t')\left(\frac{\hbar}{i}\frac{\delta}{\delta\varphi_-(t')}+\tilde{J}_+(t')+\alpha_1K_+(t')\right)+\frac{1}{2}\left(\frac{\hbar}{i}\frac{\delta}{\delta\varphi_+(t)}+J_-(t)+\alpha_1K_-(t)\right)K^{(++)}(t,t')\times\left(\frac{\hbar}{i}\frac{\delta}{\delta\varphi_+(t')}+J_-(t')+\alpha_1K_-(t')\right)\right\}, \tag{3.13}$$

$$S_2[K,\varphi]=\frac{i}{\hbar}\int_{t_I}^{\infty}dt\left\{K_+(t)\alpha_2\varphi_-(t)\varphi_+(t)+K_-(t)\frac{1}{2}\alpha_2\left(\varphi_+^2(t)+\frac{1}{4}\varphi_-^2(t)\right)+\cdots\right\}. \tag{3.14}$$

Here we introduced the function $\tilde{J}_+(t)$ as

$$\tilde{J}_+(t)=J_+(t)+\int_{t_I}^{\infty}dt'D^{(+-)-1}(t-t')Q_0\times\cos\tilde{\Omega}(t'-t_I), \tag{3.15}$$

where

$$D^{(+-)}(t-t')=\theta(t-t')\frac{\sin\tilde{\Omega}(t-t')}{M\tilde{\Omega}}, \tag{3.16}$$

and the "renormalized" frequency $\tilde{\Omega}$ is defined by

$$M\tilde{\Omega}^2=M\Omega^2+\sum_i\frac{c_i^2}{m_i\omega_i^2}. \tag{3.17}$$

The propagator for the total Hamiltonian, $K^{(+\pm)}$, is expressed in the Laplace representation form as

$$K^{(+-)}(z)=\int_0^{\infty}d(t-t')K^{(+-)}(t-t')\mathrm{e}^{-z(t-t')}=\left\{M(z^2+\Omega^2)+\sum_i\frac{c_i^2}{m_i\omega_i^2}\frac{z^2}{z^2+\omega_i^2}\right\}^{-1}, \tag{3.18}$$

$$K^{(++)}(z,z')=\int_0^{\infty}d(t-t_I)\int_0^{\infty}d(t'-t_I)\times\mathrm{e}^{-z(t-t_I)}\mathrm{e}^{-z'(t'-t_I)}K^{(++)}(t,t')=\left\{\left(i\hbar a+\frac{iM^2}{4a\hbar}zz'\right)+\sum_i c_i^2G_i^{(++)}(z,z')\right\}K^{(+-)}(z)K^{(+-)}(z'). \tag{3.19}$$

The spectral distribution function, $I(\omega)$, is formally defined by $I(\omega)=\pi\Sigma_i(c_i^2/2m_i\omega_i)\delta(\omega-\omega_i)$, which describes the character of the heat bath. In the following, we consider the Ohmic dissipation, $I(\omega)=M\gamma\omega$, where the constant γ corresponds to the strength of the damping. With the aid of Eq. (3.18), the propagator $K^{(+-)}(t-t')$ is written as

$$K^{(+-)}(t-t')=\theta(t-t')\frac{1}{M\zeta}\times\exp\left(-\frac{\gamma(t-t')}{2}\right)\sin(\zeta(t-t')), \tag{3.20}$$

where $\zeta\equiv\sqrt{\Omega^2-\gamma^2/4}$.

Setting $J=K=0$, the time evolution of the expectation value of $\hat{Q}$ in the Ohmic dissipation case is calculated from Eqs. (3.12), (3.15), and (3.20) as

$$Q_+^{(0)}(t)\equiv\langle\hat{Q}_+\rangle_t|_{J=K=0}=\left.\frac{\delta W}{\delta J_-(t)}\right|_{J=K=0}$$
$$=\left.\int_{t_I}^{\infty}dt'(K^{(+-)}(t,t')\tilde{J}_+(t')+K^{(+-)}(t,t')J_-(t'))\right|_{J=K=0}$$
$$=Q_0\theta(t-t_I)\mathrm{e}^{-(\gamma/2)(t-t_I)}\left(\frac{\Omega}{\zeta}\right)\cos\phi(t), \qquad (3.21)$$

where

$$\cos\phi_0=\frac{\zeta}{\Omega}, \qquad (3.22)$$

$$\sin\phi_0=\frac{\gamma}{2\Omega}, \qquad (3.23)$$

$$\phi(t)=\zeta(t-t_I)+\phi_0. \qquad (3.24)$$

The above equation describes a damped oscillator of the wave packet in the harmonic potential started from the position $Q_+^{(0)}(t_I)=Q_0$.

The higher-order response functions are derived by using the Feynman rule given in Appendix B that is derived from the generating functional $W[J,K]$. The Feynman role provides the way of generalizing Brownian dynamics, for example, to take into account the anharmonicity of potential. In accordance with Eqs. (3.4), (B2), and (B3), the $\alpha_1^2\alpha_2^{N-1}$- and $\alpha_1\alpha_2^N$-terms of the $(2N+1)$th-order response functions ($N=1,2$), i.e., the third- and fifth-order response functions, for $T_i>0$ ($i=1,\ldots,N$) and $\tau-t_I>0$ are given by

$$R^{(3)}(T_1;\tau)=(\alpha_1+\alpha_2Q_+^{(0)}(\tau+T_1))K^{(+-)}(T_1)\times(\alpha_1+\alpha_2Q_+^{(0)}(\tau_2)), \qquad (3.25)$$

$$R^{(5)}(T_1,T_2;\tau)=\alpha_2(\alpha_1+\alpha_2Q_+^{(0)}(T_1+T_2+\tau))\times K^{(+-)}(T_2)K^{(+-)}(T_1)(\alpha_1+\alpha_2Q_+^{(0)}(\tau))$$
$$+\alpha_2(\alpha_1+\alpha_2Q_+^{(0)}(T_1+\tau))K^{(+-)}(T_2)\times K^{(+-)}(T_1+T_2)(\alpha_1+\alpha_2Q_+^{(0)}(\tau)). \qquad (3.26)$$

Using Eq. (3.21), the response functions are expressed by the initial displacement Q_0 which corresponds to the amplitude of oscillation and the phase of the wave packet oscillator at the time τ, $\phi(\tau)$. Note that if Q_0 is replaced by $-Q_0$, the phase $\phi(\tau)$ in Eqs. (3.25) and (3.26) becomes by $\phi(\tau)+\pi$, i.e., the negative displacement leads to the phase shift of the signal. Physically one can more easily understand the effects of nonequilibrium initial condition by introducing the position and momentum at the time $t=\tau$ instead of Q_0 and $\phi(\tau)$. We also introduce $Q_\tau\equiv Q_+^{(0)}(\tau)$ and $P_\tau\equiv M(dQ_+^{(0)}(\tau)/d\tau)$, where τ implies the time when the first pump pulses interact with the system. From Eq. (3.21), we have

$$Q_+^{(0)}(t+T)=Q_\tau\left(\mathrm{e}^{-(\gamma/2)T}\cos(\zeta T)+\frac{M\gamma}{2}K^{(+-)}(T)\right)+P_\tau K^{(+-)}(T), \qquad (3.27)$$

for $T>0$ and $\tau-t_I>0$. With the use of Eq. (3.27), we have

$$R^{(3)}(T_1;\tau)=\alpha_1^2K^{(+-)}(T_1)+\alpha_1\alpha_2\left[Q_\tau\left(\mathrm{e}^{-(\gamma/2)T_1}\cos(\zeta T_1)+\frac{M\gamma}{2}K^{(+-)}(T_1)+1\right)+P_\tau K^{(+-)}(T_1)\right]K^{(+-)}(T_1), \qquad (3.28)$$

$$R^{(5)}(T_2,T_1;\tau)=\alpha_1^2\alpha_2(K^{(+-)}(T_1)K^{(+-)}(T_2)+K^{(+-)}(T_1+T_2)K^{(+-)}(T_2))$$
$$+\alpha_1\alpha_2^2\{Q_\tau[M\gamma K^{(+-)}(T_1+T_2)K^{(+-)}(T_1)K^{(+-)}(T_2)+(1+\mathrm{e}^{-(\gamma/2)(T_1+T_2)}\cos[\zeta(T_1+T_2)])$$
$$\times K^{(+-)}(T_1)K^{(+-)}(T_2)+(1+\mathrm{e}^{-(\gamma/2)T_1}\cos(\zeta T_1))\times K^{(+-)}(T_1+T_2)K^{(+-)}(T_2)]+2P_\tau K^{(+-)}(T_1+T_2)K^{(+-)}(T_1)K^{(+-)}(T_2)\}. \qquad (3.29)$$

In the same manner, we express the seventh-order response as a function of Q_τ and P_τ as follows. The seventh-order Raman response function is temporally three-dimensional but up to now only temporally two-dimensional seventh-order experiments have been performed. In the Raman echo the second propagation time T_2 is zero whereas in Raman pump–probe experiment the time variable T_1 is zero. When we set T_1 to be zero, the response function is expressed as

$$R^{(7)}(T_3,T_2,0;\tau)=2\alpha_2^2(\alpha_1+\alpha_2Q_\tau)^2K^{(+-)}(T_2)K^{(+-)}\times(T_3)K^{(+-)}(T_2+T_3), \qquad (3.30)$$

with the use of Eqs. (3.4) and (B4). This indicates that the signal in terms of T_2 and T_3 does not depend on P_τ. If we set T_2 to zero, $K^{(+-)}(T_2)$ vanishes in Eq. (B4) and the seventh-order response function is reduced to

$$R^{(7)}(T_3,0,T_1;\tau)=2\alpha_1^2\alpha_2^2K^{(+-)}(T_1)(K^{(+-)}(T_3))^2+2\alpha_1\alpha_2^3\left[Q_\tau\left(\mathrm{e}^{-(\gamma/2)T_1}\cos(\zeta T_1)+\frac{M\gamma}{2}K^{(+-)}(T_1)+1\right)+P_\tau K^{(+-)}(T_1)\right]\times K^{(+-)}(T_1)(K^{(+-)}(T_3))^2. \qquad (3.31)$$

From Eqs. (3.28) and (3.31), we find that $R^{(7)}(T_3,0,T_1;\tau)=2\alpha_2^2R^{(3)}(T_1;\tau)(K^{(+-)}(T_3))^2$. The $\alpha_1^2\alpha_2^{N-1}$-terms in $R^{(2N+1)}$ are independent of the wave packet motion and are the contribution for the equilibrium initial condition, i.e., $\hat{\rho}_I=e^{-\beta\hat{H}}/\mathrm{Tr}\,e^{-\beta\hat{H}}$. On the other hand, the $\alpha_1\alpha_2^N$-terms in $R^{(2N+1)}$ are contribution of the wave packet motion at time τ and are functions of Q_τ and P_τ. In Eqs. (3.28), (3.29), and (3.31), the response functions do not depend on the initial width of the wave packet and the temperature. As we show in Eqs. (B2), (B3), and (B4), signals depend on these higher than the terms proportional to α_2^{N+1}.

IV. NUMERICAL RESULT

In this paper, we consider the Raman experiment for a nonequilibrium initial condition set at $t=t_I$ by the Gaussian wave packet with the displacement Q_0, and the observation is started at $t=\tau$ by the irradiation of the pair of pump pulses to the system. From a different point of view, this situation can be regarded as the third-, fifth-, and seventh-order Raman experiments that provide the observation of the wave packet whose ''initial'' coordinate and ''initial'' momentum are given by Q_τ and P_τ at $t=\tau$.

In this section the third-, fifth-, and seventh-order response functions of off-resonant Raman process are numerically calculated for the Ohmic dissipation model for different coordinate Q_τ and momentum P_τ.

We set $\Omega=1000[\mathrm{cm}^{-1}]$ which is the typical value for molecular vibrational motion and $\gamma/\Omega=0.1$ (underdamped case). Taking $\tau\to\infty$, Q_τ and P_τ vanish as can be seen from Eq. (3.21) and $P_\tau=dQ_\tau/d\tau$. Then the $(2N+1)$th-order response functions approach to the equilibrium ones whose leading contribution is given by the $\alpha_1^2\alpha_2^{N-1}$-order term of $R^{(2N+1)}$, as seen from Eqs. (3.28), (3.29), and (3.31). In order to see the roles of Q_τ and P_τ that characterize the state at $t=\tau$, we plot

$$R_{\mathrm{NE}}^{(2N+1)}(T_N,\ldots,T_2,T_1;Q_\tau,P_\tau) \equiv R^{(2N+1)}(T_N,\ldots,T_2,T_1;\tau) - R^{(2N+1)}(T_N,\ldots,T_2,T_1;\infty). \tag{4.1}$$

Hereafter, we employ the dimensionless coordinate and momentum defined by $\overline{Q}_\tau\equiv\alpha_2Q_\tau/\alpha_1$ and $\overline{P}_\tau\equiv\alpha_2P_\tau/(\alpha_1M\Omega)$.

We first plot the imaginary part of the Fourier transform of the third-order Raman response function,

$$R^{(3)}(\omega;\tau)\equiv\int_0^\infty dT_1e^{i\omega T_1}R^{(3)}(T_1;\tau). \tag{4.2}$$

As a reference, in Fig. 4, we present the signal $\mathrm{Im}\,R^{(3)}(\omega;\infty)$. Figure 5 shows the imaginary part of $R_{NE}^{(3)}(\omega;Q_\tau,P_\tau)$ for $\gamma/\Omega=0.1$ for (a) $-0.01<\overline{Q}_\tau<0.01$ with $\overline{P}_\tau=0$ and (b) $-0.01<\overline{P}_\tau<0.01$ with $\overline{Q}_\tau=0$.

To understand the position of the resonant peak, it is helpful to use energy level diagrams. For the third order Raman spectroscopy, we show some representative diagrams in Fig. 6. In these diagrams, time runs horizontally from the left to the right. The vibrational states are denoted as $|v\rangle$ with $v=0,1,\ldots$. From $\hat{Q}\propto\hat{a}+\hat{a}^\dagger$, where $\hat{a}$ and $\hat{a}^\dagger$ are annihilation and creation operators ($\hat{a}^\dagger|v\rangle=\sqrt{v+1}|v+1\rangle$, $\hat{a}|v\rangle=\sqrt{v}|v-1\rangle$), we have $2^j\times2^k$ diagrams for $\alpha_j\alpha_k\langle[\hat{Q}^j(\tau+T_1),\hat{Q}^k(\tau)]\rangle$, which consist of j arrows at the time $t=\tau+T_1$ and k arrows at $t=\tau$. The upward and downward arrows stand for the transition $|v\rangle\to|v+1\rangle$ created by $\hat{a}^\dagger$ and $|v\rangle\to|v-1\rangle$ by $\hat{a}$, respectively. First, we should notice that the displaced Gaussian wave packet that we observe at $t=\tau$ involves the off-diagonal elements in the energy level representation, i.e., $\hat{\rho}_\tau=\Sigma_{v,w}\rho_{vw}|v\rangle\langle w|$ with $\rho_{vw}\neq0$ for $v\neq w$. Here $\hat{\rho}_\tau$ is a density matrix at the time $t=\tau$ defined as $\hat{\rho}_\tau=e^{-i\hat{H}(\tau-t_I)/\hbar}\hat{\rho}_Ie^{i\hat{H}(\tau-t_I)/\hbar}$. The existence of the off-diagonal elements can be understood in the following way. Any state at $t=\tau$ in the present study can be expressed in the phase space as

$$\rho_\tau\propto e^{-a\{(Q-Q_0\cos\phi)^2+[P/(M\Omega)+Q_0\sin\phi]^2\}}, \tag{4.3}$$

where ϕ is the phase determined by the ratio of Q_τ and P_τ. This state can be generated from the Gaussian wave packet $\rho_0\propto e^{-a[Q^2+(P/M\Omega)^2]}$ by the unitary transformation $\hat{D}=e^{-iQ_0(M\Omega\sin\phi\,\hat{Q}+\cos\phi\,\hat{P})}$ as $\hat{\rho}_\tau=\hat{D}\hat{\rho}_0\hat{D}^\dagger$, since $\hat{D}^\dagger\hat{Q}\hat{D}=\hat{Q}+Q_0\cos\phi$ and $\hat{D}^\dagger\hat{P}\hat{D}=\hat{P}-M\Omega Q_0\sin\phi$. Thus in the energy level representation, we have

$$\hat{\rho}_\tau=\sum_{n,m}e^{-i\phi(n-m)}\sum_l\rho_{l,l}^0D_{m,l}^{(0)}(D_{n,l}^{(0)})^*|n\rangle\langle m|, \tag{4.4}$$

where $D_{m,l}^{(0)}=\langle m|\hat{D}|l\rangle|_{\phi=0}$, because $\hat{D}=e^{\sqrt{M\Omega/2\hbar}(e^{-i\phi}\hat{a}^\dagger-e^{i\phi}\hat{a})}$ and $\hat{\rho}_0=\Sigma_l\rho_{l,l}^0|l\rangle\langle l|$. The above equation clearly indicates the existence of the off-diagonal elements.

Figure 6(a) shows the diagram for the term $\alpha_1^2\langle[\hat{Q}(\tau+T_1),\hat{Q}(\tau)]\rangle$. The laser interaction with the linear polarizability, $\alpha_1\hat{Q}\propto\alpha_1(\hat{a}+\hat{a}^\dagger)$, changes the vibrational state of the system from $|v\rangle$ to $|v\pm1\rangle$. Note that $[\hat{Q}(\tau+T_1),\hat{Q}(\tau)]$ is the c-number corresponding to the function $K^{(+-)}(T_1)$. Figures 6(b) and 6(c) show the diagrams for $\alpha_1\alpha_2\langle[\hat{Q}(\tau+T_1),\hat{Q}^2(\tau)]\rangle$ and $\alpha_1\alpha_2\langle[\hat{Q}^2(\tau+T_1),\hat{Q}(\tau)]\rangle$, respectively. The laser interaction with the nonlinear polarizability $\alpha_2\hat{Q}^2\propto\alpha_2(\hat{a}+\hat{a}^\dagger)^2$ changes the vibrational state from $|v\rangle$ to $|v\pm2\rangle$, whereas $\alpha_1\hat{Q}$ changes the state from $|v\rangle$ to $|v\pm1\rangle$.

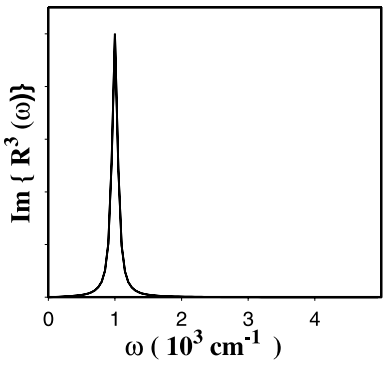

FIG. 4. Plot of the spectral density of the third-order Raman response $\mathrm{Im}\,R^{(3)}(\omega;\tau\to\infty)$, for $\gamma=0.1\Omega$.

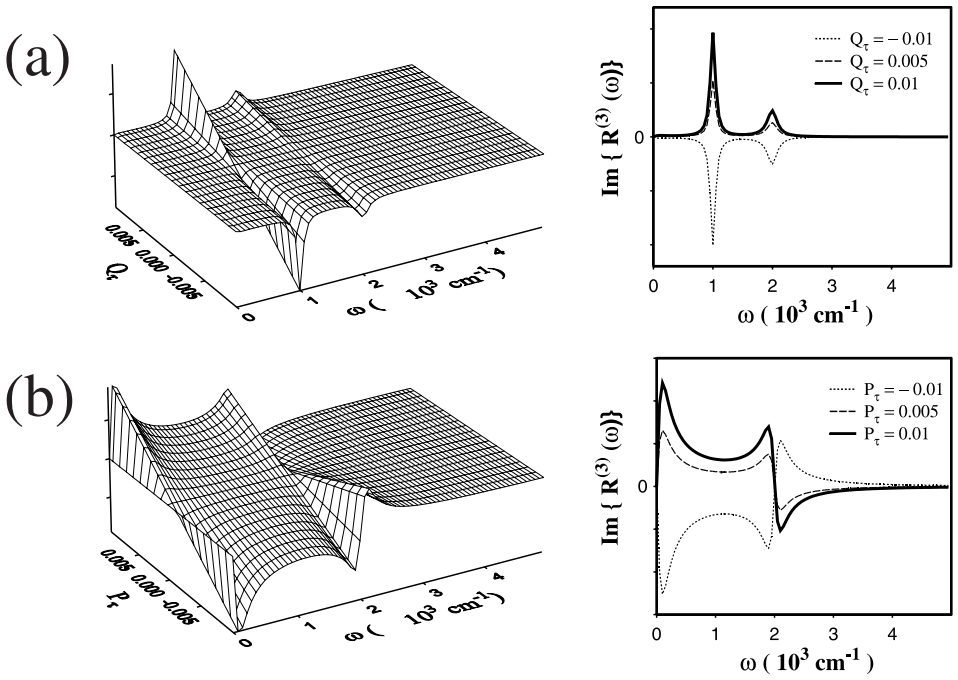

FIG. 5. Three-dimensional profile of the spectral density of the third-order Raman response, $\mathrm{Im}\, R^{(3)}_{\mathrm{NE}}(\omega;\tau)$, in the underdamped case ($\gamma=0.1\Omega$) for (a) $-0.01<\bar{Q}_\tau<0.01$, $\bar{P}_\tau=0$ and (b) $\bar{Q}_\tau=0$, $-0.01<\bar{P}_\tau<0.01$. The graph in the right is the spectral density for (a) $(\bar{Q}_\tau,\bar{P}_\tau)=(-0.01,0)$ (dotted line), $(\bar{Q}_\tau,\bar{P}_\tau)=(0.005,0)$ (dashed line), and $(\bar{Q}_\tau,\bar{P}_\tau)=(0.01,0)$ (solid line), and (b) $(\bar{Q}_\tau,\bar{P}_\tau)=(0,-0.01)$ (dotted line), $(\bar{Q}_\tau,\bar{P}_\tau)=(0,0.005)$ (dashed line), and $(\bar{Q}_\tau,\bar{P}_\tau)=(0,0.01)$ (solid line).

Because of the off-diagonal elements of wave packet at $t=\tau$, the diagrams with the different initial vibrational state and the final vibrational state can contribute to the signal. It increases linearly with $\bar{Q}_\tau$ or $\bar{P}_\tau$ due to the contribution of the off-diagonal element of the state, $\rho_{v,v\pm1}$. For negative $\bar{Q}_\tau$ and $\bar{P}_\tau$, the signal has the opposite sign, which can be seen from Eq. (4.4) by setting $\phi\rightarrow\phi+\pi$. For fixed $P_\tau=0$ in Fig. 5(a), the spectrum shows the two peaks at $\omega=\zeta\simeq\Omega$ and $\omega=2\zeta\simeq2\Omega$ with width $\gamma/2$ and γ, while for fixed $Q_\tau=0$ in Fig. 5(b), the spectrum does not show the clear peak and the spectral line changes the sign at $\omega=0$ and $\omega\simeq2\Omega$. These features can be explained clearly by using the diagram Figs. 6(b) and 6(c). With the aid of the relation $\langle[\hat{Q}(\tau+T_1),\hat{Q}^2(\tau)]\rangle=\langle\hat{Q}(\tau)[\hat{Q}(\tau+T_1),\hat{Q}(\tau)]\rangle+\langle[\hat{Q}(\tau+T_1),\hat{Q}(\tau)]\hat{Q}(\tau)\rangle$, the diagram Fig. 6(b) can be divided into two parts denoted by the dashed circle and dotted one. The contribution of the dashed part that represents $[\hat{Q}(\tau+T_1),\hat{Q}(\tau)]$ is the same as Fig. 6(a). The contribution of the dotted part gives the factor $\langle\hat{Q}(\tau)\rangle=Q_\tau$ which is related to $\rho_{v,v\pm1}$. Then Fig. 6(b) leads the Q_τ dependence and contributes to Fig. 5(a). The frequency of the signal oscillation derived from Fig. 6(b) is $\omega=\Omega$ due to the transition $|v+2\rangle\rightarrow|v+1\rangle$ at the time $t=\tau+T_1$. The signal dependence on the displacement Q_τ and the momentum P_τ can be understood from the diagram Fig. 6(c) as follows. In Fig. 6(c), the process can be divided into the two parts due to the relation $\langle[\hat{Q}^2(\tau+T_1),\hat{Q}(\tau)]\rangle=2\langle\hat{Q}(\tau+T_1)\rangle[\hat{Q}(\tau+T_1),\hat{Q}(\tau)]$. The contribution encircled by dashed line is the same as Fig. 6(a), whereas the contribution encircled by dotted line is the same as $Q_{\tau+T_1}$. By using $\hat{Q}(\tau+T)=e^{i\hat{H}T/\hbar}\hat{Q}(\tau)e^{-i\hat{H}T/\hbar}\sim\cos(\Omega\tau)\hat{Q}(\tau)+M\Omega\sin(\Omega\tau)\hat{P}(\tau)$, we find that this contribution depends on both Q_τ and P_τ. Therefore Fig. 6(c) leads to the signal in Fig. 5. Figures 5(a) and 5(b) correspond to the imaginary and real parts of $R^{(3)}(\omega)$, respectively. This is because the matrix elements involved in Fig. 6(c) are $\rho_{v,v+1}$ and, from Eq. (4.4), we have the relation $\rho^{(a)}_{v,v\pm1}=e^{\pm i\pi/2}\rho^{(b)}_{v,v\pm1}$ for the element in the case (a) and (b) that correspond to $\phi=0$ and $\phi=-\pi/2$. The signals in Fig. 5 show the oscillation with the frequency 2Ω due to the transition $|v\rangle\rightarrow|v+2\rangle$ at the time $\tau+T_1$ [using $\hat{a}^\dagger(t)\sim e^{i\Omega t}\hat{a}^\dagger$]. Their line shapes are expressed by the superposition of the two signals whose line shapes are given by the replacement of Ω, γ in $R^{(3)}(\omega;\infty)$ by 0, 2γ and 2Ω, 2γ, respectively.

Figures 7 and 8 illustrate the fifth-order Raman signal

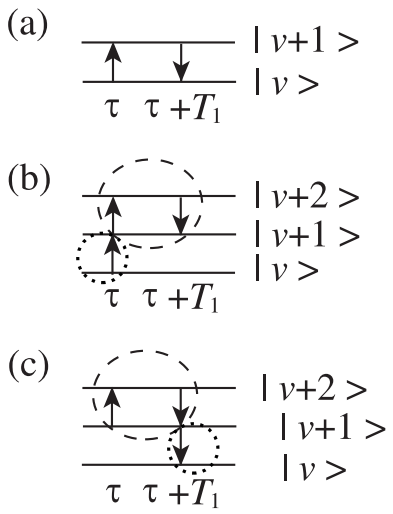

FIG. 6. Examples of the energy level diagrams associated with the third-order response function are shown. The vibrational states are denoted as $|v\rangle$, $|v+1\rangle$, and $|v+2\rangle$. (a) represents the $\alpha_1^2\langle[\hat{Q}(\tau+T_1),\hat{Q}(\tau)]\rangle$. (b) and (c) correspond to $\alpha_1\alpha_2\langle[\hat{Q}(\tau+T_1),\hat{Q}^2(\tau)]\rangle$ and $\alpha_1\alpha_2\langle[\hat{Q}^2(\tau+T_1),\hat{Q}(\tau)]\rangle$. The contribution of the dashed part that represents $[\hat{Q}(\tau+T_1),\hat{Q}(\tau)]$ is the same as the diagram (a). The contribution of the dotted part gives the factor $\langle\hat{Q}(\tau)\rangle=Q_\tau$.

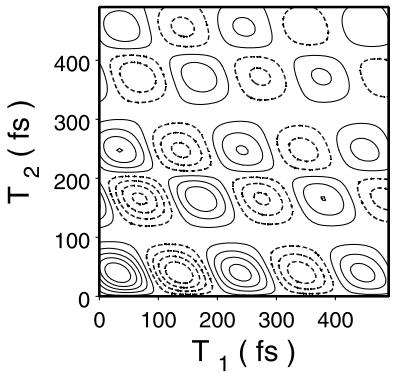

FIG. 7. Contour plot of the equilibrium part of the fifth-order Raman response, $I^{(5)}(T_1,T_2;\infty)=R^{(5)}(T_2,T_1;\tau\rightarrow\infty)$, in the underdamped case ($\gamma=0.1\Omega$). Dashed contours are negative.

$I^{(5)}(T_1,T_2;\tau)=R^{(5)}(T_2,T_1;\tau)$ calculated from Eq. (3.29) for the damping constant $\gamma/\Omega=0.1$. Figure 7 is the equilibrium part $R^{(5)}(T_2,T_1;\infty)$, whereas Figs. 8(a), 8(b), and 8(c) depict the nonequilibrium part $R^{(5)}_{\rm NE}(T_2,T_1;Q_\tau,P_\tau)$ for (a) $\overline{Q}_\tau=0$, $\overline{P}_\tau=0.01$, (b) $\overline{Q}_\tau=0.01$, $\overline{P}_\tau=0$, and (c) $\overline{Q}_\tau=5\times10^{-3}$, $\overline{P}_\tau=-8.66\times10^{-3}$. Their phase $\phi(\tau)$ correspond to (a) $\phi(\tau)=-\pi/2$, (b) $\phi(\tau)=0$, and (c) $\phi(\tau)=\pi/3$, respectively. The signal $R^{(5)}(T_2,T_1,\tau)$ vanishes at $T_2=0$ in all the cases Figs. 7 and 8(a)–8(c) as can be seen from the definition, Eq. (2.8). The fifth-order response function is diagrammatically expressed in Fig. 9. In the diagrams for $\alpha_j\alpha_k\alpha_l\langle[[\hat{Q}^j(\tau+T_1+T_2),\hat{Q}^k(\tau+T_1)],\hat{Q}^l(\tau)]\rangle$, j, k, and l, arrows are depicted at the time $t=\tau+T_1+T_2$, $\tau+T_1$, and τ, respectively. The α_1^3-terms are canceled out by each other because of the commutation relation in $[[\hat{Q},\hat{Q}],\hat{Q}]$. The leading order terms are therefore $\alpha_1{}^2\alpha_2\langle[[\hat{Q}^2,\hat{Q}],\hat{Q}]\rangle$ and $\alpha_1{}^2\alpha_2\langle[[\hat{Q},\hat{Q}^2],\hat{Q}]\rangle$ and are shown in Figs. 9(a) and 9(b), respectively. These diagrams lead the signal in Fig. 7. According to the commutation relation $[[\hat{Q}^2(\tau+T_1+T_2),\hat{Q}(\tau+T_1)],\hat{Q}(\tau)]=2[\hat{Q}(\tau+T_1+T_2),\hat{Q}(\tau+T_1)][\hat{Q}(\tau+T_1+T_2),\hat{Q}(\tau)]$, Fig. 9(a) is represented by the product of two parts, a-1 and a-2, which are associated with the third order response function $[\hat{Q}(\tau+T_1+T_2),\hat{Q}(\tau+T_1)]\sim K^{(+-)}(T_2)$ and $[\hat{Q}(\tau+T_1+T_2),\hat{Q}(\tau)]\sim K^{(+-)}(T_1+T_2)$, respectively; it shows the oscillation with the frequency 2Ω along T_2 direction. In the same manner, Fig. 9(b) is represented by the product of two processes b-1 and b-2 that are associated with $K^{(+-)}(T_1)$ and $K^{(+-)}(T_2)$, respectively; it shows the oscillation with the frequency Ω in both the T_1 and T_2 direction. Therefore we have the signals with the frequency Ω in the T_1 direction and the frequency Ω and 2Ω in the T_2 direction in the $\alpha_1^2\alpha_2$-order. The frequencies in the $\alpha_1\alpha_2^2$-order terms can be understood with the use of the diagrams Figs. 9(c) and 9(d) which correspond to $\alpha_1\alpha_2^2\langle[[\hat{Q}^2,\hat{Q}],\hat{Q}^2]\rangle$ and $\alpha_1\alpha_2^2\langle[[\hat{Q},\hat{Q}^2],\hat{Q}^2]\rangle$, respectively. These diagrams have the same frequencies as Figs. 9(a) and 9(b) and are independent of the momentum P_τ, since they can be divided into the dashed circle of Fig. 9(c), that of Fig. 9(d), and the dotted circles of Figs. 9(c) and 9(d), which correspond to the diagrams Figs. 9(a), 9(b), and Q_τ, respectively. The dependence of P_τ is derived from the remaining term $\alpha_1\alpha_2^2\langle[[\hat{Q}^2,\hat{Q}^2],\hat{Q}]\rangle$. Using the commutation relation, the

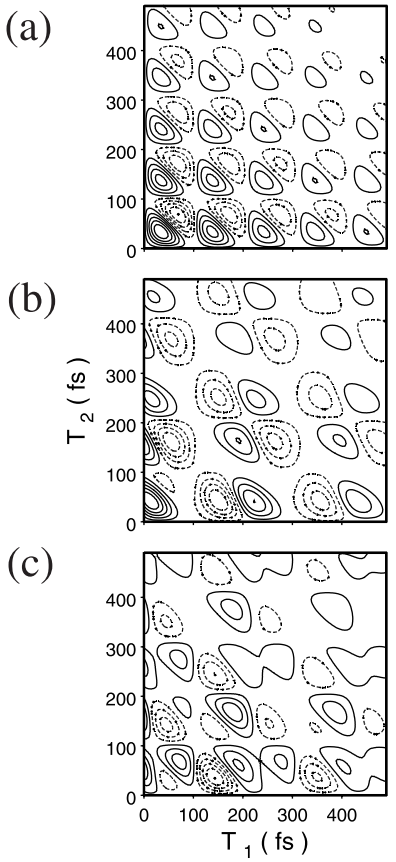

FIG. 8. Contour plot of the fifth-order Raman response $R^{(5)}_{\rm NE}(T_2,T_1)$ in the underdamped case ($\gamma=0.1\Omega$) for (a) $(\overline{Q}_\tau,\overline{P}_\tau)=(0,0.01)$, (b) $(\overline{Q}_\tau,\overline{P}_\tau)=(0.01,0)$, and (c) $(\overline{Q}_\tau,\overline{P}_\tau)=(5\times10^{-3},-8.66\times10^{-3})$. Dashed contours are negative.

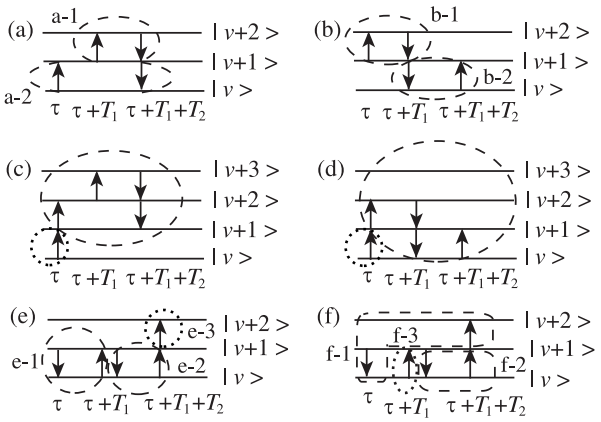

FIG. 9. Examples of the energy level diagrams associated with the fifth-order response function are shown. The vibrational states are denoted as $|v\rangle$, $|v+1\rangle$, $|v+2\rangle$, and $|v+3\rangle$. (a) and (b) correspond to $\alpha_1^2\alpha_2\langle[[\hat{Q}^2,\hat{Q}],\hat{Q}]\rangle$ and $\alpha_1^2\alpha_2\langle[[\hat{Q},\hat{Q}^2],\hat{Q}]\rangle$. (c) and (d) are $\alpha_1\alpha_2{}^2\langle[[\hat{Q}^2,\hat{Q}],\hat{Q}^2]\rangle$, $\alpha_1\alpha_2{}^2\langle[[\hat{Q},\hat{Q}^2],\hat{Q}^2]\rangle$, respectively. The contribution of the dashed parts in (c) and (d) are the same as the diagrams (a) and (b), whereas the dotted parts in (c) and (d) give the factor $\langle\hat{Q}(\tau)\rangle=Q_\tau$. Using Eq. (4.5), the term $\alpha_1\alpha_2{}^2\langle[[\hat{Q}^2,\hat{Q}^2],\hat{Q}]\rangle$ is divided in the two parts expressed by (e) and (f).

term $\alpha_1\alpha_2^2\langle[[\hat{Q}^2,\hat{Q}^2],\hat{Q}]\rangle$ is rewritten in two terms as follows,

$$\alpha_1\alpha_2^2\langle[[\hat{Q}^2(\tau+T_1+T_2),\hat{Q}^2(\tau+T_1)],\hat{Q}(\tau)]\rangle$$
$$=2\alpha_1\alpha_2^2\langle\hat{Q}(\tau+T_1+T_2)[\hat{Q}(\tau+T_1+T_2),\hat{Q}(\tau+T_1)]$$
$$\times[\hat{Q}(\tau+T_1),\hat{Q}(\tau)]\rangle+2\alpha_1\alpha_2^2\langle[\hat{Q}(\tau+T_1+T_2),$$
$$\hat{Q}(\tau)][\hat{Q}(\tau+T_1+T_2),\hat{Q}(\tau+T_1)]\hat{Q}(\tau+T_1)\rangle. \quad (4.5)$$

The diagrams Fig. 9(e) and 9(f) correspond to the first and the second term of Eq. (4.5). From Eq. (3.27), $Q_{\tau+T_1+T_2}$ and $Q_{\tau+T_1}$ are expressed in terms of Q_τ and P_τ, which means that the signals depend on both the position and the momentum at the time τ. The product of e-1, e-2, and e-3 in Fig. 9(e) or that of f-1, f-2, and f-3 in Fig. 9(f) shows the oscillation with frequency 2Ω along T_1 and T_2. From the above discussion, we can understand the profile of the signals for different parameters. In Fig. 7, the signal oscillates with the frequency Ω in the T_1 direction and Ω and 2Ω in the T_2 direction as discussed in Figs. 9(a) and 9(b). In Fig. 8(a), the signal oscillates with the frequency 2Ω in the T_1 and the T_2 direction, which is attributed to the zero quantum transitions $|v\rangle\rightarrow|v\rangle$ at the time $t=\tau+T_1$ and the two quantum transition $|v\rangle\rightarrow|v+2\rangle$ at the time $t=\tau+T_1+T_2$ shown in Figs. 9(e) and 9(f). In Fig. 8(a), the signal is symmetric with respect to T_1 and T_2 axis since the diagrams Figs. 9(e) and 9(f) cast into the form $P_\tau K^{(+-)}(T_1+T_2)K^{(+-)}(T_1)K^{(+-)}(T_2)$ with the use of the relations $Q_{\tau+T_1+T_2}=P_\tau K^{(+-)}(T_1+T_2)$ and $Q_{\tau+T_1}=P_\tau K^{(+-)}(T_1)$ for $Q_\tau=0$, which is derived from Eq. (3.27). The signal in Fig. 8(b) includes various components corresponding to the diagrams in Figs. 9(c), 9(d), 9(e), and 9(f) that lead the oscillations with the frequency Ω and 2Ω in the T_1 and T_2 direction with the different weight depending on a condition at $t=\tau$ and as a consequence, the signal is asymmetric. In Fig. 8(c), the signal consists of the $\overline{P}_\tau$ and $\overline{Q}_\tau$ contribution which are depicted in Figs. 8(a) and 8(b) with the ratio $-\sin\phi(\tau)$ to $\cos\phi(\tau)$. A profile of any signal in the present model can be characterized by the phase $\phi(\tau)$. Thus, by obtaining a proper $\phi(\tau)$ to simulate experimental data, we can trace the motion of the wave packet at $t=\tau$ moved from the initial state at $t=t_I$. The main advantage of the present method is that, by measuring the signal for different τ, we can directly trace the time evolution of the wave packet in the phase space, i.e., we can obtain the momentum and the coordinate of the wave packet at once. Note that, although the same argument can be applied to the third-order response, the higher-order response that leads the two-dimensional profile reveals the more critical information.

Finally, we plot the seventh-order signal, $I^{(7)}(T_1,T_3;\tau)=R^{(7)}(T_3,T_2=0,T_1;\tau)$ calculated from Eq. (3.31) for $\gamma/\Omega=0.1$. The equilibrium part $I^{(7)}(T_1,T_3;\infty)$ is given in Fig. 10. The nonequilibrium parts, $I^{(7)}_{\mathrm{NE}}(T_1,T_3;Q_\tau,P_\tau)=R^{(7)}_{\mathrm{NE}}(T_3,0,T_1;Q_\tau,P_\tau)$, for (a) $\overline{Q}_\tau=0$, $\overline{P}_\tau=0.01$, (b) $\overline{Q}_\tau=0.01$, $\overline{P}_\tau=0$, and (c) $\overline{Q}_\tau=5\times10^{-3}$, $\overline{P}_\tau=-8.66\times10^{-3}$ which correspond to the phase (a) $\phi(\tau)=-\pi/2$, (b) $\phi(\tau)=0$, and (c) $\phi(\tau)=\pi/3$ are given in Figs. 11(a), 11(b), and 11(c), respectively. Figures 12(a)–12(e) represent the diagrams corresponding to $\alpha_1^2\alpha_2^2\langle[[[\hat{Q}^2,\hat{Q}^2],\hat{Q}],\hat{Q}]\rangle$, $\alpha_1^2\alpha_2^2\langle[[[\hat{Q}^2,\hat{Q}],\hat{Q}^2],\hat{Q}]\rangle$, $\alpha_1\alpha_2^3\langle[[[\hat{Q}^2,\hat{Q}^2],\hat{Q}],\hat{Q}^2]\rangle$, $\alpha_1\alpha_2^3\langle[[[\hat{Q}^2,\hat{Q}],\hat{Q}^2],\hat{Q}^2]\rangle$, and $\alpha_1\alpha_2^3\langle[[[\hat{Q}^2,\hat{Q}^2],\hat{Q}^2],\hat{Q}]\rangle$, respectively. Each of them is expressed by the product of circled parts, which lead to the third-order correlation function $K^{(+-)}$ and Q_τ and P_τ. Using the similar manipulation as in the fifth-order case, the diagrams in Figs. 12(a)–12(d) lead to the oscillation with frequency Ω in the T_1 direction

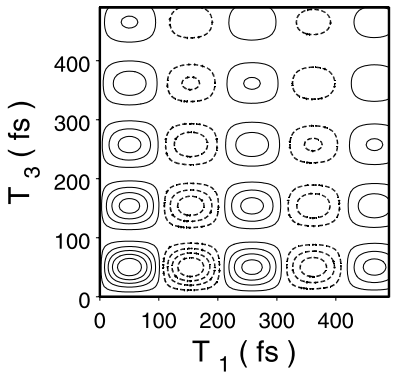

FIG. 10. Contour plot of the equilibrium part of the seventh-order Raman response, $I^{(7)}(T_1,T_3;\infty)=R^{(7)}(T_3,T_1;\tau\rightarrow\infty)$, in the underdamped case ($\gamma=0.1\Omega$). Dashed contours are negative.

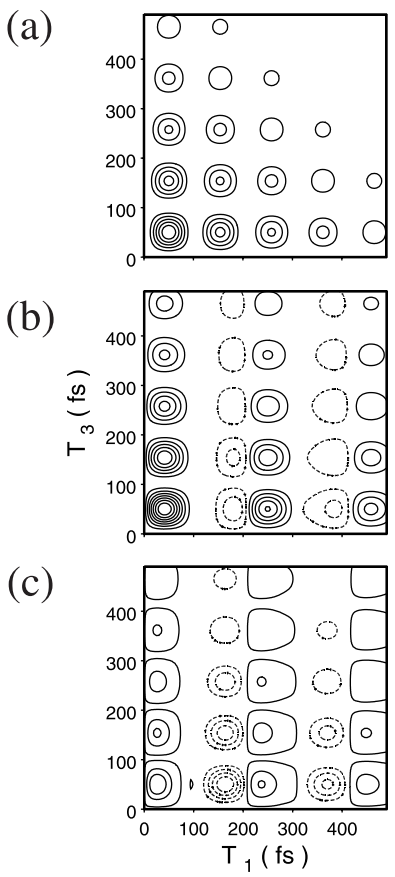

FIG. 11. Contour plot of the seventh-order Raman response $R^{(7)}_{\mathrm{NE}}(T_3,T_1)$ in the underdamped case ($\gamma=0.1\Omega$) for (a) $(\overline{Q}_\tau,\overline{P}_\tau)=(0,0.01)$, (b) $(\overline{Q}_\tau,\overline{P}_\tau)=(0.01,0)$, and (c) $(\overline{Q}_\tau,\overline{P}_\tau)=(5\times10^{-3},-8.66\times10^{-3})$. Dashed contours are negative.

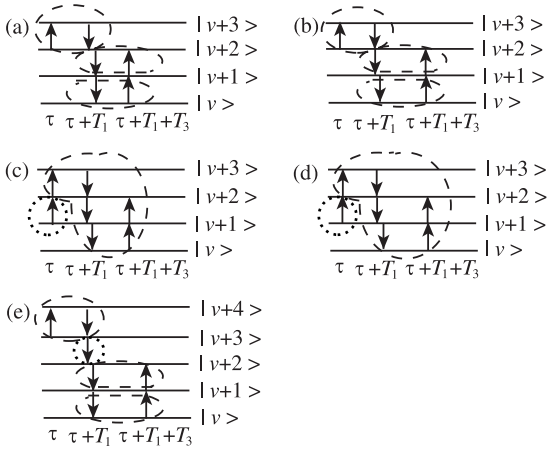

FIG. 12. Examples of the energy level diagrams associated with the seventh-order response function at $T_2=0$ are shown. The vibrational states are denoted as $|v\rangle$, $|v+1\rangle$, $|v+2\rangle$, $|v+3\rangle$, and $|v+4\rangle$. (a) and (b) correspond to $\alpha_1^2\alpha_2^2\langle[[[\hat{Q}^2,\hat{Q}^2],\hat{Q}],\hat{Q}]\rangle$ and $\alpha_1^2\alpha_2^2\langle[[[\hat{Q}^2,\hat{Q}],\hat{Q}^2],\hat{Q}]\rangle$. (c), (d), and (e) correspond to $\alpha_1\alpha_2^3\langle[[[\hat{Q}^2,\hat{Q}^2],\hat{Q}],\hat{Q}^2]\rangle$, $\alpha_1\alpha_2^3\langle[[[\hat{Q}^2,\hat{Q}],\hat{Q}^2],\hat{Q}^2]\rangle$, and $\alpha_1\alpha_2^3\langle[[[\hat{Q}^2,\hat{Q}^2],\hat{Q}^2],\hat{Q}]\rangle$, respectively. The contribution of the dashed parts in (c) and (d) are the equivalent to the diagrams (a) and (b), whereas the dotted parts in (c) and (d) give the factor Q_τ.

and 2Ω in the T_3 direction, and the diagram in Fig. 12(e) leads to the oscillation with the frequency 2Ω both in the T_1 and T_3 direction. Then we observe the oscillation Ω in the T_1 direction and 2Ω in the T_2 direction in Fig. 10, since only the diagrams in Figs. 12(a) and 12(b) contribute to the equilibrium signal. In the case Fig. 11(a), we observe the oscillation 2Ω both T_1 and T_3 direction, since the process corresponding to Fig. 12(e) contributes to the signal. In the case Fig. 11(b), the diagram Figs. 12(c)–12(e) contribute to the signal. Hence the oscillation in the T_1 direction and that in the T_3 direction becomes by the superposition of the oscillations with the frequencies Ω and 2Ω. The signal in Fig. 11(c) is given by the linear combination of the signals in Figs. 11(a) and 11(b) with the ratio $-\sin\phi(\tau)$ to $\cos\phi(\tau)$. This situation is same as the fifth-order case and we can use the seventh-order experiment to see the dynamics of the wave packet in the phase space, as well.

V. CONCLUSION

In this paper, we derived the generating functional for a Brownian oscillator system whose initial state is described by displaced Gaussian wave packet from the path integral approach. The generating functional allows for the calculation of the third-, fifth-, seventh-order Raman response of a harmonic oscillator with coordinate dependence of the polarizability. To demonstrate effects of the nonequilibrium initial condition, we plot the Raman response for the different displacement and momentum of the wave packet at the time $t=\tau$ when the first pump pulses interact with the system. Any state at time τ can be expressed by a Gaussian wave packet centered at $P_\tau/(M\Omega)=-A\sin\phi$ and $Q_\tau=A\cos\phi$, where A and ϕ are the amplitude and the phase in the phase space and are given by $A=Q_0$ and $\phi=\Omega\tau$ for an oscillator with frequency Ω. Due to the off-diagonal elements of the state at $t=\tau$, the signals depend on the wave packet motion and show the mode with the frequency 2Ω which does not appear in the equilibrium case. In the third order response, the signal decays with decreasing the displacement Q_τ for the positive displacement ($\phi=0$) and it increases with decreasing $|Q_\tau|$ for the negative displacement ($\phi=\pi$). Consequently, the time evolution of the signal implies whether the wave packet is displaced initially toward decreasing or increasing bond length. In the fifth- (seventh-) order response, the component of the signal which is proportional to P_τ is symmetry with respect to T_1 and T_2 (T_1 and T_3). On the other hand, the component which is proportional to Q_τ is asymmetric. These properties can be explained with the help of the energy level diagrams. In the signal, the ratio of a Q_τ contribution to a $P_\tau/(M\Omega)$ contribution is $\cos\phi$ to $-\sin\phi$. Thus, by looking for the phase ϕ to simulate experimental data, we can trace the motion of the wave packet at time $t=\tau$ moved from the initial state at time $t=0$. The main advantage of the present method is that we can obtain the information about not only the position but also the momentum of the wave packet.

In the present studies, we restricted our analysis to the order of $\alpha_1^2\alpha_2^{N-1}$ and $\alpha_1\alpha_2^N$, so the response functions do not depend on the initial width of the wave packet and the temperature as stated in Sec. III; the dependence of the temperature and the width of the wave packet appear in the order of α_2^{N+1}. Such effects as well as the effects of the anharmonicity of an oscillation mode may be studied from the equation of motion approach.[17,33,34]

ACKNOWLEDGMENTS

The authors thank professor Hiro-o Hamaguchi mentioning about a possibility to use 2D spectroscopy to detect the phase of the wave packet motion. The present investigations were supported by the Grant-in-Aid on Priority Area of Chemical Reaction Dynamics in Condensed Phases (10206210), the Grant-in-Aid for Scientific Research (B)(12440171).

APPENDIX A: DERIVATION OF THE GENERATING FUNCTIONAL

In this Appendix, we derive the generating functional $W[J,K]$ defined by Eq. (3.2) for the initial state Eqs. (3.7)–(3.10). By integrating over the bath coordinate $\mathbf{q}_I$ and $\mathbf{q}_I'$, $W[J,K]$ is given by

$$\exp\left(\frac{i}{\hbar}W[J,K]\right)=\left[\prod_i\frac{1}{2\sinh\dfrac{\beta\hbar\omega_i}{2}}\right]\times\exp\left[\frac{i}{\hbar}\frac{1}{2}\sum_i\int_{C_1+C_2}dtdt'\times\left(\frac{\hbar}{i}\frac{\delta}{\delta_C J(t)}\right)c_i^2G_C^{(m_i,\omega_i)}(t,t')\times\left(\frac{\hbar}{i}\frac{\delta}{\delta_C J(t')}\right)\right]\exp\left(\frac{i}{\hbar}W_S[J,K]\right),\tag{A1}$$

where

$$\exp\left(\frac{i}{\hbar}W_S[J,K]\right)$$
$$=\int dQ_I\int dQ_I'\langle Q_I'|\rho_I^{(S)}|Q_I\rangle$$
$$\times\langle Q_I|\hat{U}_{S2}^{\dagger}(t_F,t_I)\hat{U}_{S1}(t_F,t_I)|Q_I'\rangle, \tag{A2}$$

$$\hat{U}_{S\alpha}(t,t')=\mathrm{T}\exp\left\{\frac{i}{\hbar}\int_{t'}^{t}ds\left(\frac{\hat{P}^2}{2M}+\frac{1}{2}M\tilde{\Omega}^2\hat{Q}^2\right.\right.$$
$$\left.\left.-J_\alpha(s)\hat{Q}-K_\alpha(s)\alpha(\hat{Q})\right)\right\}\ (\alpha=1,2), \tag{A3}$$

$$G_C^{(m,\omega)}(t,t')=\frac{i}{2m\omega}\frac{1}{\sinh\frac{\hbar\beta\omega}{2}}$$
$$\times\left\{\theta_C(t-t')\cos\left[\omega\left(t-t'+\frac{i\beta\hbar}{2}\right)\right]\right.$$
$$\left.+\theta_C(t'-t)\cos\left[\omega\left(t'-t+\frac{i\beta\hbar}{2}\right)\right]\right\}. \tag{A4}$$

Here $\tilde{\Omega}$ is given in Eq. (3.17). Notice that we take the final time t_F to be set infinity in the end of this Appendix. The functional differentiation $\delta/\delta_C J(t)$ means $\delta/\delta J_1(t)$ and $-\delta/\delta J_2(t)$ for $t\in C_1$ and $t\in C_2$, respectively.

The factor $\langle Q_I'|\hat{U}_{S2}^{\dagger}(t_F,t_I)\hat{U}_{S1}(t_F,t_I)|Q_I\rangle$ is calculated as follows. Inserting the completeness relation $1=\int dQ_F|Q_F\rangle\langle Q_F|$ at the final time t_F, we have

$$\langle Q_I'|\hat{U}_{S2}^{\dagger}(t_F,t_I)\hat{U}_{S1}(t_F,t_I)|Q_I\rangle$$
$$=\int dQ_F\langle Q_I'|\hat{U}_{S2}^{\dagger}(t_F,t_I)|Q_F\rangle\langle Q_F|\hat{U}_{S1}(t_F,t_I)|Q_I\rangle. \tag{A5}$$

The time evolution kernel with the sources J_1,K_1, $\langle Q_F|\hat{U}_{S1}(t_F,t_I)|Q_I\rangle$ is given by (see, for example, Ref. 35)

$$\langle Q_F|\hat{U}_{S1}(t_F,t_I)|Q_I\rangle$$
$$=\left(\frac{M\tilde{\Omega}}{2\pi i\hbar\sin\tilde{\Omega}T}\right)^{1/2}$$
$$\times\exp\left\{-\frac{i}{\hbar}\int_{t_I}^{t_F}dsV\left(\frac{\hbar}{i}\frac{\delta}{\delta J_1(s)};K_1(s)\right)\right\}$$
$$\times\exp\left[\frac{i}{\hbar}\left\{\frac{1}{2}\int_{t_I}^{t_F}dt\int_{t_I}^{t_F}dt'J_1(t)\Delta(t,t')J_1(t')\right.\right.$$
$$+Q_I\int_{t_I}^{t_F}dt\frac{\sin\tilde{\Omega}(t_F-t)}{\sin\tilde{\Omega}T}J_1(t)$$
$$+Q_F\int_{t_I}^{t_F}dt\frac{\sin\tilde{\Omega}(t-t_I)}{\sin\tilde{\Omega}T}J_1(t)-\frac{M\tilde{\Omega}}{\sin\tilde{\Omega}T}Q_IQ_F$$
$$\left.\left.+\frac{M\tilde{\Omega}}{2}\frac{\cos\tilde{\Omega}T}{\sin\tilde{\Omega}T}(Q_F^2+Q_I^2)\right\}\right], \tag{A6}$$

where

$$V(Q;K(s))=-K(s)\alpha(Q), \tag{A7}$$

$$\Delta(t,t')=-\frac{1}{M\tilde{\Omega}}\left[\theta(t-t')\frac{\sin\tilde{\Omega}(t'-t_I)\sin\tilde{\Omega}(t_F-t)}{\sin\tilde{\Omega}T}\right.$$
$$\left.+\theta(t'-t)\frac{\sin\tilde{\Omega}(t-t_I)\sin\tilde{\Omega}(t_F-t')}{\sin\tilde{\Omega}T}\right]. \tag{A8}$$

The kernel of the return path with the source J_2 and K_2, denoted by $\langle Q_I|\hat{U}_{S2}(t_I,t_F)|Q_F\rangle$, is given by replacing J_1 and K_1 with J_2 and K_2 for the complex conjugate of Eq. (A6). By integrating over Q_F, Eq. (A8) is expressed as

$$\int dQ_F\langle Q_I'|\hat{U}_{J_2}^{\dagger}(t_F,t_I)|Q_F\rangle\langle Q_F|\hat{U}_{J_1}(t_F,t_I)|Q_I\rangle \tag{A9}$$
$$=\exp\left[-\frac{i}{\hbar}\int_{t_I}^{t_F}ds\left\{V\left(\frac{\hbar}{i}\frac{\delta}{\delta J_1(s)};K_1(s)\right)\right.\right.$$
$$\left.\left.-V\left(\frac{-\hbar}{i}\frac{\delta}{\delta J_2(s)};K_2(s)\right)\right\}\right]$$
$$\times\delta\left((Q_I-Q_I')-\int_{t_I}^{t_F}dtD^{(+-)}(t-t_I)\right)$$
$$\times\exp\left\{\frac{i}{\hbar}\left(\frac{Q_I+Q_I'}{2}\int_{t_I}^{t_F}dt\cos\Omega(t-t_I)J_-(t)\right.\right.$$
$$\left.\left.+\int_{t_I}^{t_F}dt\int_{t_I}^{t_F}dt'J_-(t)D^{(+-)}(t-t')J_+(t')\right)\right\}, \tag{A10}$$

where $J_\pm$ is defined by Eq. (3.11). Choosing the displaced Gaussian wave packet (3.10) as the initial state, $W_S[J,K]$ is calculated by integrating over (Q_I-Q_I') and $(Q_I+Q_I')/2$ as

$$\exp\left(\frac{i}{\hbar}W_S[J,K]\right)$$
$$=\exp\left[-\frac{i}{\hbar}\int_{t_I}^{t_F}ds\left\{V\left(\frac{\hbar}{i}\frac{\delta}{\delta J_1(s)};K_1(s)\right)\right.\right.$$
$$\left.\left.-V\left(\frac{-\hbar}{i}\frac{\delta}{\delta J_2(s)};K_2(s)\right)\right\}\right]$$
$$\times\exp\left\{\frac{i}{\hbar}\int_{t_I}^{t_F}dt\int_{t_I}^{t_F}dt'J_-(t)(D^{(+-)}(t-t')J_+(t')\right.$$
$$+Q_0\cos\Omega(t-t_I)\delta(t-t'))$$
$$\left.+\frac{i}{2\hbar}\int_{t_I}^{t_F}dt\int_{t_I}^{t_F}dt'J_-(t)D^{(++)}(t,t')J_-(t')\right\}. \tag{A11}$$

Here $D^{(+-)}$ and $D^{(++)}$ are the propagators without coupling to the bath and are given by Eq. (3.16) and

$$D^{(++)}(t,t')=\frac{\hbar}{i}\left(-aD^{(+-)}(t-t_I)D^{(+-)}(t'-t_I)\right.$$
$$\left.-\frac{1}{4a\hbar^2}\cos\tilde{\Omega}(t-t_I)\cos\tilde{\Omega}(t'-t_I)\right), \tag{A12}$$

$$1=\exp\left(\frac{i}{\hbar}\int_{C_1+C_2}dtJ(t)\varphi(t)\right)\Bigg|_{\varphi=0}=\exp\left(\frac{i}{\hbar}\int_{t_I}^{t_F}dt(J_+(t)\varphi_-(t)+J_-(t)\varphi_+(t))\right)\Bigg|_{\varphi=0} \tag{A13}$$

from the right-hand side of Eq. (A1), and using the relation $e^{F_1[\delta/\delta J]}e^{F_2[J]}e^{\int dsJ(s)\varphi(s)}\big|_{\varphi=0}=e^{F_2[J+\delta/\delta\varphi]}e^{F_1[\varphi]}\big|_{\varphi=0}$, we obtain the following result:

$$\begin{aligned}\exp\left(\frac{i}{\hbar}W[J,K]\right)=&\left[\prod_i\frac{1}{2\sinh\dfrac{\beta\hbar\omega_i}{2}}\right]\exp\left[\frac{i}{\hbar}\int_{t_I}^{t_F}dt\int_{t_I}^{t_F}dt'\left(\frac{\hbar}{i}\frac{\delta}{\delta\varphi_+(t)}+J_-(t)\right)\right.\\&\times\left\{D^{(+-)}(t-t')\left(\frac{\hbar}{i}\frac{\delta}{\delta\varphi_-(t)}+J_+(t)\right)+Q_0\cos\tilde{\Omega}(t-t_I)\delta(t-t')\right\}\\&\left.+\frac{i}{2\hbar}\int_{t_I}^{t_F}dt\int_{t_I}^{t_F}dt'\left(\frac{\hbar}{i}\frac{\delta}{\delta\varphi_+(t)}+J_-(t)\right)D^{(++)}(t,t')\left(\frac{\hbar}{i}\frac{\delta}{\delta\varphi_+(t')}+J_-(t')\right)\right]\\&\times\exp\left[\frac{i}{2\hbar}\sum_i\int_{t_I}^{t_F}dt\int_{t_I}^{t_F}dt'\{\varphi_-(t)(c_i^2G_i^{(++)}(t,t'))\varphi_-(t')+\varphi_-(t)(c_i^2G_i^{(+-)}(t-t'))\varphi_+(t')\}\right]\\&\times\exp\left[-\frac{i}{\hbar}\int_{t_I}^{t_F}ds\{V(\varphi_1(s);K_1(s))-V(\varphi_2(s);K_2(s))\}\right]\Bigg|_{\varphi=0},\end{aligned} \tag{A14}$$

where

$$G_i^{(+-)}(t-t')\equiv G_{11}^{(m_i,\omega_i)}(t,t')-G_{12}^{(m_i,\omega_i)}(t,t')=\theta(t-t')\frac{1}{m_i\omega_i}\sin\omega_i(t-t'), \tag{A15}$$

$$G_i^{(++)}(t,t')\equiv\frac{1}{4}(G_{11}^{(m_i,\omega_i)}(t,t')+G_{12}^{(m_i,\omega_i)}(t,t')+G_{21}^{(m_i,\omega_i)}(t,t')+G_{22}^{(m_i,\omega_i)}(t,t'))=\frac{i}{2m_i\omega_i}\coth\left(\frac{\beta\hbar\omega_i}{2}\right)\cos\omega_i(t-t'). \tag{A16}$$

Equation (A14) leads to the Feynman rule described in Fig. 13. Using this rule, $W[J,K]$ can be cast into the following form:

$$\begin{aligned}\exp\left(\frac{i}{\hbar}W[J,K]\right)=&\left[\prod_i\frac{1}{2\sinh\dfrac{\beta\hbar\omega_i}{2}}\right]\exp\left[\frac{i}{\hbar}\int_{t_I}^{t_F}dt\int_{t_I}^{t_F}dt'\left\{\left(\frac{\hbar}{i}\frac{\delta}{\delta\varphi_+(t)}+J_-(t)\right)K^{(+-)}(t-t')\left(\frac{\hbar}{i}\frac{\delta}{\delta\varphi_-(t')}+\tilde{J}_+(t')\right)\right.\right.\\&\left.\left.+\frac{1}{2}\left(\frac{\hbar}{i}\frac{\delta}{\delta\varphi_+(t)}+J_-(t)\right)K^{(++)}(t,t')\left(\frac{\hbar}{i}\frac{\delta}{\delta\varphi_+(t')}+J_-(t')\right)\right\}\right]\\&\times\exp\left[-\frac{i}{\hbar}\int_{t_I}^{t_F}ds\{V(\varphi_1(s);K_1(s))-V(\varphi_2(s);K_2(s))\}\right]\Bigg|_{\varphi=0}.\end{aligned} \tag{A17}$$

Here $K^{(+-)}$ and $K^{(++)}$ are the propagators for the system including the effects of the bath. By using the fact that $K^{(+-)}(t-t')$ is causal, we can find the graphical expression Fig. 14 from the Feynman rule Fig. 13. The algebraic expression of Fig. 14 is represented as

$$\begin{aligned}K^{(+-)}(t-t')=&D^{(+-)}(t-t')+\int_{t_I}^{t_F}ds\int_{t_I}^{t_F}ds'D^{(+-)}(t-s)\left(\sum_i c_i^2G_i^{(+-)}(s-s')\right)D^{(+-)}(s'-t')\\&+\int_{t_I}^{t_F}ds\int_{t_I}^{t_F}ds'\int_{t_I}^{t_F}ds''\int_{t_I}^{t_F}ds'''D^{(+-)}(t-s)\left(\sum_i c_i^2G_i^{(+-)}(s-s')\right)D^{(+-)}(s'-s'')\\&\times\left(\sum_i c_i^2G_i^{(+-)}(s''-s''')\right)D^{(+-)}(s'''-t')\cdots.\end{aligned} \tag{A18}$$

Summing up the right-hand side of Fig. 14, we have the following relation:

$$K^{(+-)}(t-t') = D^{(+-)}(t-t') + \int_{t_I}^{t_F} ds \int_{t_I}^{t_F} ds' D^{(+-)}(t-s) \times \left(\sum_i c_i^2 G_i^{(+-)}(s-s') \right) K^{(+-)}(s'-t'). \tag{A19}$$

Using the Laplace transformation, $K^{(+-)}$ in $t_F \to \infty$ is represented as

$$K^{(+-)}(z) = D^{(+-)}(z) + D^{(+-)}(z) \times \left(\sum_i c_i^2 G_i^{(+-)}(z) \right) K^{(+-)}(z), \tag{A20}$$

where $D^{(+-)}(z)$ and $G_i^{(+-)}(z)$ are given by

$$D^{(+-)}(z) = \frac{1}{M} \frac{1}{z^2 + \tilde{\Omega}^2}, \tag{A21}$$

$$G_i^{(+-)}(z) = \frac{1}{m_i} \frac{1}{z^2 + \omega_i^2}. \tag{A22}$$

This leads the expression in Eq. (3.18).

Next, $K^{(++)}(t,t')$ can be obtained in the same manner. The algebraic expression of $K^{(++)}$ is

$$\begin{aligned} K^{(++)}(t,t') = {} & D^{(++)}(t,t') + \int_{t_I}^{t_F} ds \int_{t_I}^{t_F} ds' D^{(++)}(t,s) \\ & \times \left(\sum_i c_i^2 G_i^{(-+)}(s-s') \right) K^{(-+)}(s'-t') \\ & + \int_{t_I}^{t_F} ds \int_{t_I}^{t_F} ds' D^{(+-)}(t-s) \\ & \times \left(\sum_i c_i^2 G_i^{(+-)}(s-s') \right) K^{(++)}(s',t') \\ & + \int_{t_I}^{t_F} ds \int_{t_I}^{t_F} ds' D^{(+-)}(t-s) \\ & \times \left(\sum_i c_i^2 G_i^{(++)}(s,s') \right) K^{(-+)}(s'-t'), \end{aligned} \tag{A23}$$

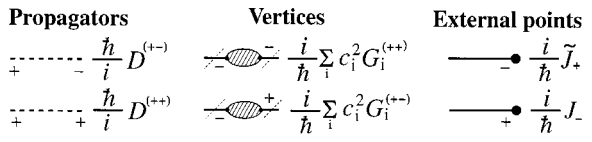

FIG. 13. Feynman rule.

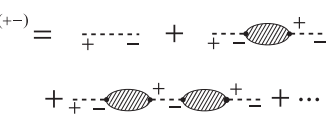

FIG. 14. Diagrammatical expression of a propagator $K^{(+-)}$.

where $G_i^{(-+)}(t-t') \equiv G_i^{(+-)}(t'-t)$, $K^{(-+)}(t-t') \equiv K^{(+-)}(t'-t)$ and another propagators $D^{(++)}(t,t')$ and $G_i^{(++)}(t,t')$ are given by Eqs. (A12) and (A16), respectively. Now, we take the final time $t_F \to \infty$. Using the first line of Eq. (3.18) and substituting Eqs. (A12) and (A16) into Eq. (A23), we obtain the propagator $K^{(++)}$ as in Eq. (3.19).

Applying the relation,

$$e^{F[\delta/\delta\varphi]} e^{\int ds K(s)\varphi(s)} = e^{\int ds K(s)\varphi(s)} e^{F[(\delta/\delta\varphi)+K]}, \tag{A24}$$

to Eq. (A17), we arrive at the result given in Eq. (3.12).

APPENDIX B: DERIVATION OF *N* TIME CORRELATION FUNCTION BY USE OF FEYNMAN RULES

In this Appendix, we present the Feynman rules that lead the N time correlation functions, $G_R^{(N+1)}$, defined by Eq. (3.5). From Eqs. (3.5) and (3.14), we have following rules:

(1) Prepare $N+1$ white circles corresponding to $\alpha_{k_0}, \alpha_{k_1}, \ldots,$ and α_{k_N} ($k_i = 1,2\ldots$; $i = 0,1,\ldots,N$). The white circle corresponding to α_{k_i} from which k_i lines emerge shall be called the external point;
(2) Prepare black circles corresponding to sources $\tilde{J}_+^{(0)}$ that are treated as one-point vertices. A line emerges from this black circle;
(3) Attach a time valuable t_0 to the external point corresponding to α_{k_0}. We call it an external point labeled t_0;
(4) Attach a time valuable t_i to the external point corresponding to α_{k_i}. We call it an external point labeled t_i;
(5) Attach a time valuable t to a black circle corresponding to $\tilde{J}_+^{(0)}$;
(6) Prepare lines corresponding to propagators, $K^{(+\pm)}$;
(7) Attach the index "+" or "−" to each line from an external point or a black circle as in Fig. 15.
The factors on the right of the graphs imply attachments to the graphs.
(8) Using the propagators, external points, and one-point vertices, draw all connected diagrams which are topologically distinct. Note here that the diagram which contains the propagators connecting the indices "−" and "−" are excluded;
(9) Carry out the integration over all internal time from t_I to ∞;
(10) Multiply the contribution of each diagram by $(\hbar/i)^{N+1}/S$, where S is the symmetry factor. The symmetry factor S is defined as the order of the permutation group of the internal lines and vertices leaving the diagram unchanged when the external lines are fixed.

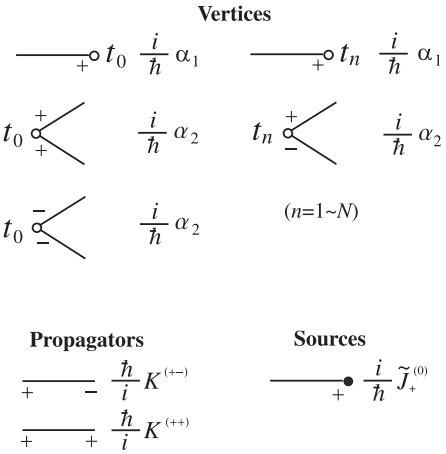

FIG. 15. Feynman rule for response functions.

As an example, let us consider the second-order correlation function, $G_R^{(2)}(t_0,t_1)$. In accordance with the above rules, $G_R^{(2)}(t_0,t_1)$ is diagrammatically given by Fig. 16(a) after introducing the expression

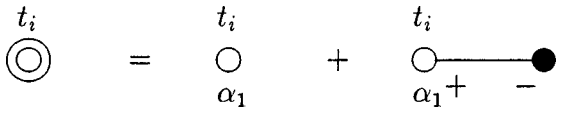

$$= \frac{i}{\hbar}\left(\alpha_1 + \alpha_2 \int_{t_I}^{\infty} ds K^{(+-)}(t-s)\tilde{J}_+^{(0)}(s) \right)$$

$$= \frac{i}{\hbar}(\alpha_1 + \alpha_2 Q_+^{(0)}(t)), \tag{B1}$$

where the last equation is obtained with the use of the second line of Eq. (3.21). Following to the rules, we can write down the analytical expression in the form

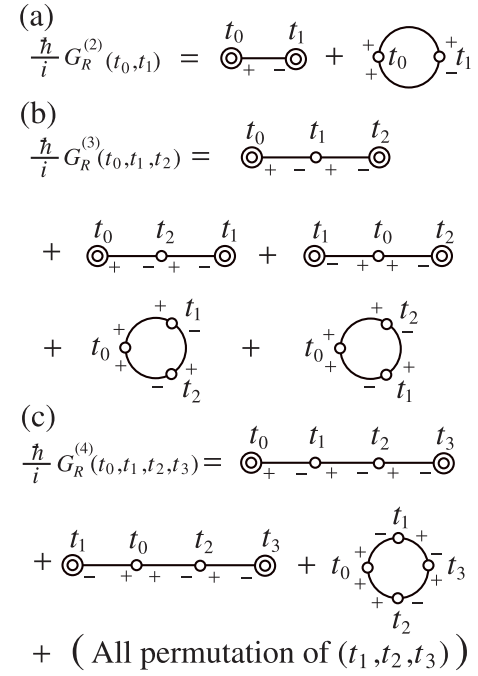

FIG. 16. Diagrammatical representation of (a) second-, (b) third-, and (c) fifth-order response functions expressed by the terms Eq. (B1) and Fig. 15.

$$\frac{i}{\hbar}G_R^{(2)}(t_0,t_1) = (\alpha_1 + \alpha_2 Q_+^{(0)}(t_0))K^{(+-)}(t_0-t_1)(\alpha_1 + \alpha_2 Q_+^{(0)}(t_1)) + \alpha_2^2 \frac{i}{\hbar}K^{(++)}(t_0,t_1)K^{(+-)}(t_0-t_1) + \cdots. \tag{B2}$$

In the same way, the third-order correlation function, $G_R^{(3)}(t_0,t_1,t_2)$, and the fourth order correlation function, $G_R^{(4)}(t_0,t_1,t_2,t_3)$, are diagrammatically expressed as in Figs. 16(b) and 16(c), respectively. Then the analytical expression for these diagrams are given by

$$\left(\frac{i}{\hbar}\right)^2 G_R^{(3)}(t_0,t_1,t_2) = (\alpha_1 + \alpha_2 Q_+^{(0)}(t_0))\alpha_2 K^{(+-)}(t_0-t_1)K^{(+-)}(t_1-t_2)(\alpha_1 + \alpha_2 Q_+^{(0)}(t_2)) + (t_1 \leftrightarrow t_2) + (\alpha_1 + \alpha_2 Q_+^{(0)}(t_1))\alpha_2 K^{(-+)}(t_1-t_0)K^{(+-)}(t_0-t_2)(\alpha_1 + \alpha_2 Q_+^{(0)}(t_2)) + \frac{i}{\hbar}\alpha_2^3 (K^{(++)}(t_0,t_1) \times K^{(+-)}(t_0-t_2)K^{(+-)}(t_2-t_1) + K^{(++)}(t_0,t_2)K^{(+-)}(t_0-t_1)K^{(+-)}(t_1-t_2)) + \cdots, \tag{B3}$$

$$\left(\frac{i}{\hbar}\right)^3 G_R^{(4)}(t_0,t_1,t_2,t_3) = (\alpha_1 + \alpha_2 Q_+^{(0)}(t_0))\alpha_2^2 K^{(+-)}(t_0-t_1)K^{(+-)}(t_1-t_2)K^{(+-)}(t_2-t_3)(\alpha_1 + \alpha_2 Q_+^{(0)}(t_3)) + (5 \text{ terms that are all permutation of } (t_1,t_2,t_3)) + (\alpha_1 + \alpha_2 Q_+^{(0)}(t_1)) \times \alpha_2^2 K^{(-+)}(t_1-t_0)K^{(+-)}(t_0-t_2)K^{(+-)}(t_2-t_3)(\alpha_1 + \alpha_2 Q_+^{(0)}(t_3)) + (\text{five terms that are all permutation of } (t_1,t_2,t_3)) + \frac{i}{\hbar}\alpha_2^4 (K^{(+-)}(t_0-t_1)K^{(+-)}(t_1-t_2) \times K^{(+-)}(t_2-t_3)K^{(++)}(t_3,t_0)) + (5 \text{ terms that are all permutation of } (t_1,t_2,t_3)) + \cdots. \tag{B4}$$

[1] Y. Tanimura and S. Mukamel, J. Chem. Phys. **99**, 9496 (1993).
[2] P. Hamm, M. Lim, W. F. DeGrado, and R. M. Hochstrasser, Proc. Natl. Acad. Sci. U.S.A. **96**, 2036 (1999).
[3] V. Astinov, K. Kubarych, C. J. Milne, and R. J. D. Miller, Opt. Lett. **25**, 853 (2000).
[4] V. Astinov, K. Kubarych, C. J. Milne, and R. J. D. Miller, Chem. Phys. Lett. **327**, 334 (2000).
[5] D. A. Blank, L. J. Kaufman, and G. R. Fleming, J. Chem. Phys. **113**, 771 (2000).
[6] O. Golonzka, N. Demirdoven, M. Khalil, and A. Tokmakoff, J. Chem. Phys. **113**, 9893 (2000).
[7] L. J. Kaufman, D. A. Blank, and G. Fleming, J. Chem. Phys. **114**, 2312 (2001).
[8] W. Zhao and J. C. Wright, Phys. Rev. Lett. **83**, 1950 (1999).
[9] W. Zhao and J. C. Wright, J. Am. Chem. Soc. **121**, 10994 (1999).
[10] W. Zhao and J. C. Wright, Phys. Rev. Lett. **84**, 1411 (2000).
[11] M. C. Asplund, M. T. Zanni, and R. M. Hochstrasser, Proc. Natl. Acad. Sci. U.S.A. **97**, 8219 (2000).
[12] O. Golonzka, M. Khalil, N. Demirdoven, and A. Tokmakoff, Phys. Rev. Lett. **86**, 2154 (2001).
[13] A. Tokmakoff and G. R. Fleming, J. Chem. Phys. **106**, 2569 (1997).
[14] S. Saito and I. Ohmine, J. Chem. Phys. **108**, 240 (1998).
[15] A. Ma and R. M. Stratt, Phys. Rev. Lett. **85**, 1004 (2000).
[16] K. Okumura and Y. Tanimura, J. Chem. Phys. **106**, 1687 (1997); **107**, 2267 (1997); Chem. Phys. Lett. **277**, 159 (1997).
[17] Y. Tanimura, Chem. Phys. **233**, 217 (1998).
[18] V. Chernyak and S. Mukamel, J. Chem. Phys. **108**, 5812 (1998).
[19] S. Hahn, K. Park, and M. Cho, J. Chem. Phys. **111**, 4121 (1999).
[20] K. Park, M. Cho, S. Hahn, and D. Kim, J. Chem. Phys. **111**, 4131 (1999).
[21] K. Park and M. Cho, J. Chem. Phys. **112**, 10496 (2000).
[22] K. Okumura and Y. Tanimura, Chem. Phys. Lett. **278**, 175 (1997).
[23] K. Okumura, D. M. Jonas, and Y. Tanimura, Chem. Phys. **266**, 237 (2001).
[24] R. L. Murry, J. T. Fourkas, and T. Keyes, J. Chem. Phys. **109**, 7913 (1998).
[25] T. Key and J. T. Fourcas, J. Chem. Phys. **112**, 287 (2000).
[26] R. A. Denny and D. R. Reichman, Phys. Rev. E **63**, 065101 (2001).
[27] K. Okumura, A. Tokmakoff, and Y. Tanimura, J. Chem. Phys. **111**, 492 (1999).
[28] S. Hahn, K. Kwak, and M. Cho, J. Chem. Phys. **112**, 4553 (2000).
[29] F. Rosca, A. T. N. Kumar, X. Ye, T. Sjodin, A. A. Demidov, and P. M. Champion, J. Phys. Chem. A **2000**, 4280 (2000).
[30] A. J. Niemi and G. W. Semenoff, Ann. Phys. (N.Y.) **152**, 105 (1984); Nucl. Phys. B **230**, [FS 10] 181 (1984).
[31] M. Wagner, Phys. Rev. B **44**, 6104 (1991).
[32] R. Fukuda, M. Sumino, and K. Nomoto, Phys. Rev. A **45**, 3559 (1992); R. Fukuda and M. Sumino, *ibid.* **44**, 6252 (1991).
[33] T. Steffen and Y. Tanimura, J. Phys. Soc. Jpn. **69**, 3115 (2000).
[34] Y. Tanimura and T. Steffen, J. Phys. Soc. Jpn. **69**, 4095 (2000).
[35] R. P. Feynman and A. R. Hibbs, *Quantum Mechanics and Path Integrals* (McGraw–Hill, New York, 1965).